Geosci. Model Dev., 15, 3387–3404, 2022
https://doi.org/10.5194/gmd-15-3387-2022

Geoscientific Model Development
Open Access
EGU

Precipitation over southern Africa: is there consensus among global climate models (GCMs), regional climate models (RCMs) and observational data?

Maria Chara Karypidou[1], **Eleni Katragkou**[1], **and Stefan Pieter Sobolowski**[2]

[1]Department of Meteorology and Climatology, School of Geology, Faculty of Sciences, Aristotle University of Thessaloniki, Thessaloniki, Greece
[2]NORCE Norwegian Research Centre, Bjerknes Centre for Climate Research, Bergen, Norway

Correspondence: Maria Chara Karypidou (karypidou@geo.auth.gr)

Received: 5 March 2021 – Discussion started: 7 May 2021
Revised: 27 December 2021 – Accepted: 18 January 2022 – Published: 22 April 2022

Abstract. The region of southern Africa (SAF) is highly vulnerable to the impacts of climate change and is projected to experience severe precipitation shortages in the coming decades. Ensuring that our modeling tools are fit for the purpose of assessing these changes is critical. In this work we compare a range of satellite products along with gauge-based datasets. Additionally, we investigate the behavior of regional climate simulations from the Coordinated Regional Climate Downscaling Experiment (CORDEX) – Africa domain, along with simulations from the Coupled Model Intercomparison Project Phase 5 (CMIP5) and Phase 6 (CMIP6). We identify considerable variability in the standard deviation of precipitation between satellite products that merge with rain gauges and satellite products that do not, during the rainy season (October–March), indicating high observational uncertainty for specific regions over SAF. Good agreement both in spatial pattern and the strength of the calculated trends is found between satellite and gauge-based products, however. Both CORDEX-Africa and CMIP ensembles underestimate the observed trends during the analysis period. The CMIP6 ensemble displayed persistent drying trends, in direct contrast to the observations. The regional ensembles exhibited improved performance compared to their forcing (CMIP5), when the annual cycle and the extreme precipitation indices were examined, confirming the added value of the higher-resolution regional climate simulations. The CMIP6 ensemble displayed a similar behavior to CMIP5, but reducing slightly the ensemble spread. However, we show that reproduction of some key SAF phenomena, like the Angola Low (which exerts a strong influence on regional precipitation), still poses a challenge for the global and regional models. This is likely a result of the complex climatic processes that take place. Improvements in observational networks (both in situ and satellite) as well as continued advancements in high-resolution modeling will be critical, in order to develop a robust assessment of climate change for southern Africa.

1 Introduction

The region of Sub-Saharan Africa has been characterized as one of the most vulnerable regions to climate change (Kula et al., 2013; Serdeczny et al., 2017), and more specifically, the region of southern Africa (SAF) has been identified as a climate change hotspot (Diffenbaugh and Giorgi, 2012). Taking into consideration that the majority of the population living in SAF (70 %) is dependent on rainfed agriculture (Mabhaudhi et al., 2018), any climate-change-induced alteration of the spatiotemporal patterns of precipitation will require a rapid adaptation of the agricultural sector. Concurrently, SAF is also characterized by low adaptive capacity to changes in climatic conditions (Davis and Vincent, 2017); hence, it emerges as a high-risk region. In addition, approximately 26 % of the SAF population is undernourished (AFDB, 2019). This figure is expected to increase significantly by 2050 (Tirado et al., 2015). Apart from the impacts on the agricultural sector though, climatic changes are expected to alter the spatiotemporal patterns of vector-borne disease occurrence (Rocklöv and Dubrow, 2020), cause se-

vere damage to infrastructure and road networks (Chinowsky et al., 2015), and exacerbate poverty (Azzarri and Signorelli, 2020). Due to these impacts it is critical that the current spatiotemporal patterns of precipitation are accurately reproduced by our modeling systems and observations (whether in situ, reanalysis or satellite) over SAF. Only then can we credibly assess future climate change impacts and inform strategies aiming to mitigate their effects on local communities.

Towards this end, satellite, gauge-based and reanalysis products are extensively used, in order to monitor current spatial and temporal precipitation patterns and to further characterize precipitation variability and change during recent decades. For future projections however, climate models able to simulate the (thermo)dynamical processes of the atmosphere are employed. Such an endeavor has been performed in the context of the Coupled Model Intercomparison Project Phase 5 (CMIP5) (Taylor et al., 2012) using General Circulation Models (GCMs) and in the context of the Coordinated Regional Climate Downscaling Experiment (CORDEX) – Africa domain (Giorgi and Gutowski, 2015) using Regional Climate Models (RCMs). The latest advancement in the climate modeling community involves GCMs and Earth system models (ESMs), participating in the CMIP6 ensemble, providing input for the 6th Assessment Report of the Intergovernmental Panel on Climate Change (IPCC) (Eyring et al., 2016). However, the confidence with which one can claim future climate projections produced by GCMs, ESMs or RCMs are fit for purpose is usually assessed based on their ability to simulate current climatic conditions. For instance, Munday and Washington (2018) showed that the CMIP5 ensemble displayed a systematic wet bias over the SAF region that was caused by the misrepresentation of orographic features located over the area of Tanzania. A wet bias caused by structural model errors was also identified in the dynamically downscaled and higher-resolution CORDEX-Africa ensemble (Kim et al., 2014). Therefore, a valid question arises as to what the most suitable dataset is, with which climate impact studies can be fed when the SAF region is the focus. In addition, before the task of characterizing future precipitation trends is addressed, it is imperative to diagnose the degree to which observed precipitation trends over the recent decades are reproduced by GCMs and RCMs.

A comprehensive analysis of the performance of the CORDEX-Africa ensemble over Africa was first presented in Nikulin et al. (2012). They showed that during the rainy season (January–March as used in Nikulin et al., 2012) there is a weak wet bias over southern Africa and that the use of the ensemble mean enabled individual models to be outperformed, highlighting the importance of ensemble-based approaches. The Nikulin et al. (2012) analysis was conducted on a pan-African scale. Similarly, Kalognomou et al. (2013) analyzed the same ensemble of CORDEX-Africa simulations, focusing on southern Africa, and reported similar findings. In Meque and Abiodun (2015) the same ensemble of 10 evaluation simulations was again used, but it was also compared with a set of CMIP5 GCM simulations, with the purpose of identifying a causal association between ENSO and drought events over southern Africa. In Meque and Abiodun (2015) it was stated that RCMs were able to provide added value, compared to their driving GCMs. A comprehensive assessment of the added value between historical CORDEX-Africa RCM simulations and of their driving CMIP5 GCMs on a seasonal timescale over the whole of Africa was performed in Dosio et al. (2019). The first time the CORDEX-Africa ensemble is compared to both CMIP5 and CMIP6 ensembles is presented in Dosio et al. (2021). More specifically, in Dosio et al. (2021) the analysis is performed on a seasonal time step and on pan-African scale and its particular emphasis is placed on the projected changes of future precipitation, although a part of the analysis is dedicated to the period 1981–2010.

Satellite and gauge-based datasets display increasing trends during the historical period for annual precipitation over SAF (32–41 mm yr^{-1} per decade), an observation that is also identifiable in the Atmospheric Model Intercomparison Project (AMIP), but not in CMIP5 (Maidment et al., 2015). During DJF, precipitation trends over SAF display a remarkably robust signal in gauge-based, satellite and AMIP datasets (Maidment et al., 2015). In addition, Onyutha (2018) also reported on the increasing precipitation trends over SAF during DJF, especially after the 1960s. However, according to CMIP5, precipitation is projected to decrease over SAF in the 21st century (IPCC, 2013). This estimate also holds for simulations performed using RCMs forced with CMIP5 (Pinto et al., 2016; Dosio et al., 2019). The increase in the observed precipitation trends over SAF has been attributed to the recent strengthening of the Pacific Walker Circulation (Maidment et al., 2015), which is captured in observational datasets and in AMIP simulations, but not in CMIP5 (L'Heureux et al., 2013; Yim et al., 2016). CMIP6 displays an even more robust future decline in precipitation and increase in drought events over SAF, relative to its predecessor (Ukkola et al., 2020). However, although the CMIP6 ensemble exhibits multiple improvements on various levels (Wyser et al., 2020), certain biases and challenges identified in CMIP5 during the historical period persist in CMIP6 (Kim et al., 2020).

RCMs are known to add value to climate simulations over regional scales, mainly because the spatial resolution increases, resolving atmospheric waves in a more detailed manner, and also because surface characteristics interacting with the atmosphere are represented more accurately (Denis et al., 2003; Giorgi et al., 2014). Considering the aforementioned challenges displayed in the CMIP5 simulations to accurately capture precipitation amounts under current climatic conditions and recent precipitation trends, we investigate the degree to which this observation holds also for RCMs forced with GCMs participating in the CMIP5 ensemble. Theory tells us that RCMs develop their own physics. However, oftentimes the impact of the driving GCMs on the RCM simu-

lations is evident (Denis et al., 2003; Laprise et al., 2008; Di Luca et al., 2013; Giorgi, 2019).

Therefore, in this paper we expand on previous research to investigate how monthly precipitation during the rainy season over southern Africa is simulated by different modeling systems, by analyzing the monthly precipitation climatologies, the interannual variability, specific precipitation indices and monthly precipitation trends during the period 1986–2005, in four different modeling systems (CORDEX0.22°/0.44°, CMIP5/6) and observational ensembles (satellite, reanalysis and gridded datasets). Our main goal is to provide a comprehensive overview with regards to precipitation climatology over SAF as simulated by the state-of-the-art tools used by climate scientists. In addition, we investigate whether higher-resolution models are able to provide an improved representation of precipitation over southern Africa and we investigate how a particularly important atmospheric feature, the Angola Low (AL) pressure system, is simulated in the RCM and GCM ensembles.

In Sect. 2 the data used are presented along with the methodology employed. In Sect. 3 the results are presented. More specifically, the results are analyzed based on the monthly climatology, the annual cycle of precipitation, the AL pressure system, the precipitation indices and the monthly precipitation trends. Lastly, in Sect. 4 we provide the discussion of the analysis along with some concluding remarks.

2 Data and methodology

2.1 Data

We analyze daily and monthly precipitation from five types of datasets, namely observational datasets (OBS), GCMs and ESMs that comprise the CMIP5 and CMIP6 ensembles, and regional climate models (RCMs) that comprise the CORDEX-Africa ensemble at 0.44° of spatial resolution (CORDEX0.44) and at 0.22° of spatial resolution (CORDEX0.22). The analysis is concerned with the SAF region, which is defined as the area between 10 and 42° E and 10 to 35° S. The analyzed period is 1986–2005, as this is the period during which the estimates of all 5 aforementioned datasets overlap. Although satellite and reanalysis products cannot be termed as purely "observational", in the context of the current work they are classified as such, in order to differentiate them from climate model datasets (CORDEX0.44, CORDEX0.22, CMIP5, CMIP6). Hereafter "OBS" refers to satellite, gauge-based and reanalysis products.

2.1.1 Observational data

The OBS data used are based on the analysis of Le Coz and van de Giesen (2020) and are comprised of five gauge-based products (datasets that are derived by spatial interpolation of rain gauges and station data: CRU.v4.01, UDEL.v7, PREC/L.v0.5, GPCC.v7, CPC-Global.v1), six satellite products (given below) and one reanalysis product, ERA5. The datasets have a temporal coverage that extends through the analyzed period (1986–2005). The gauge-based products were chosen so that they have a spatial resolution less than or equal to $0.5° \times 0.5°$and the satellite products have a spatial resolution less or equal to $0.25° \times 0.25°$. For satellite products, however, there was an exception for two products (CMAP.v19.11and GPCP.v2.2) with a resolution equal to $2.5° \times 2.5°$ that were also included in the analysis due to their widespread use in the literature. The OBS ensemble is made of 12 products. More details concerning the OBS datasets are provided in Table S1 in the Supplement. In certain parts of the following analysis the OBS products are either used collectively or they are split into sub-ensembles, based on the methods used for their production. More specifically, these sub-ensembles are the mean of all gauge-based precipitation products (Gauge-Based), the ensemble mean of satellite products that merge with rain gauges (Satellite-Merge) (ARC.v2, CMAP.v19.11, GPCP.v2.2) and the ensemble mean of satellite products that do not merge directly with rain gauges (Satellite-NoMerge) (CHIRPS.v2, TAMSAT.v3, PERSIANN-CDR), but they use alternative methods such as calibration, bias adjustment or artificial neural network techniques (Le Coz and van de Giesen, 2020).

2.1.2 Climate model simulations

We retrieved daily precipitation for a set of 26 RCM simulations performed as part of CORDEX-Africa historical simulations at 0.44° (∼ 50 km) spatial resolution, comprising the CORDEX0.44 ensemble. We also retrieved a set of 10 RCM simulations performed within CORDEX-Africa, as part of the CORDEX-CORE project (Coppola et al., 2021), available at 0.22° (∼ 25 km) spatial resolution (CORDEX0.22). In addition, daily precipitation was retrieved for a set of 10 CMIP5 GCMs, with 3 additional simulations with variations in the GCM's resolution (IPSL-LR/IPSL-MR), the ocean model (GFDL-ESM2M/GFDL-ESM2G) and Realization/Initialization/Physics (ICHCE-EC-EARTH-r1i1p1/ICHCE-EC-EARTH-r12i1p1). The CMIP5 models selected were the ones used as forcing in the CORDEX0.44 historical simulations. In total, precipitation from a set of 13 CMIP5 simulations was used. Additionally, we exploited daily precipitation from a set of 8 CMIP6 GCM and ESM simulations. The CMIP6 simulations selected were performed with the updated versions of the same models that were part of the CMIP5 ensemble. This selection served to construct CMIP5 and CMIP6 ensembles that were comparable. Precipitation data for all simulations were retrieved from the Earth System Grid Federation (ESGF). In addition, we retrieved temperature at 850 hPa for both CORDEX0.44/0.22 from ESGF. For the CMIP5 and CMIP6 simulations temperature and geopotential height at 850 hPa was retrieved from the Climate Data Store (CDS). Geopotential height at

850 hPa was not available for CORDEX-Africa simulations. Lastly, elevation data for CORDEX-Africa and CMIP5 were obtained from ESGF, while the Shuttle Radar Topography Mission (SRTM) (Farr et al., 2007) digital elevation model was used as the observed elevation in the topography transects for a selected latitude over SAF. Details about the models used are provided in Tables S2–S5.

2.2 Methodology

Precipitation climatologies are investigated on a monthly basis, due to the fact that precipitation over SAF arises as the result of atmospheric mechanisms that display high variability during the rainy season. The aggregation of precipitation to seasonal means might often obscure certain spatial characteristics that are better identified on a monthly basis. The within-ensemble agreement is investigated using the sample standard deviation (SD), which is calculated using monthly mean values over the period 1986–2005 for each model (or observational dataset) separately. We also employ four precipitation indices constructed in the context of the Expert Team on Climate Change Detection and Indices (ETCCDI) (Peterson and Manton, 2008), utilizing daily precipitation amounts for the period 1986–2005. The four ETCCDI indices are used to describe total annual precipitation (PRCPTOT), annual maximum daily precipitation (Rx1Day), annual number of days with daily precipitation > 10 mm (R10mm) and annual number of days with daily precipitation > 20 mm (R20mm). These indices are calculated for each individual simulation of each ensemble (CMIP5, CMIP6, CORDEX0.44 and CORDEX0.22), and OBS products, separately and yield a value for every year (January–December) during the period 1986–2005. The calculation of indices required data with a daily temporal resolution; hence, observational datasets that provided monthly aggregates are excluded. The spatial averages calculated over SAF for the annual cycle and the ETCCDI indices consider land pixels only. For the construction of ensemble means, either in observational or model ensembles, datasets were remapped to the coarser grid using conservative remapping for precipitation and bilinear interpolation for temperature and geopotential height at 850 hPa.

In order to investigate some basic thermodynamical aspects that may differentiate precipitation in the CMIP5/6 and the CORDEX0.44/0.22 ensembles, we look into the seasonal representation of the Angola Low (AL) pressure system over SAF. The AL pressure system is a semi-permanent synoptic scale system that plays a strong role in modulating precipitation over SAF (Reason and Jagadheesha, 2005; Lyon and Mason, 2007; Crétat et al., 2019; Munday and Washington, 2017; Howard and Washington, 2018). More specifically, the reason why we chose to put an emphasis on the AL pressure system is that the AL redistributes low-tropospheric moisture entering SAF from the southern Atlantic and the southern Indian oceans and also moisture transport originating from the Congo basin. In addition, AL events precede the formation of tropical temperate troughs (TTTs) and hence, they can be considered as their precursor in the "climate process chain" (Daron et al., 2019). As stated in Howard and Washington (2018), it is common that AL events precede TTT events, since the AL pressure system functions as a key process necessary for the transport of water vapor from the tropics towards the extratropics (Hart et al., 2010).

In Munday and Washington (2017) AL events were identified using geopotential height at 850 hPa. However, since geopotential height at 850 hPa is not available for CORDEX0.44/0.22 simulations, we could not employ this method. Hence, based on the variables that are already available within both CORDEX and CMIP5/6 ensembles, we use potential temperature at 850 hPa (theta850) as an alternative "proxy" variable that provides thermodynamical information. In order to ensure that theta850 can be used instead of zg850, we examine the relationship between theta850 and zg850 over the study region in ERA5, for each month of the rainy season (October–March), using the climatological mean monthly values for the period 1986–2005 (Figs. S1, S2). As shown in Fig. S1, during October over the southeastern part of Angola, there is a region of low pressure. Moving towards the core of the rainy season, the low-pressure system deepens, while there seems to be a weak extension of low pressure towards the south. Also, as shown in Fig. S2, during October there is an area of high theta850 values located over southeastern Angola, coinciding with the region of low zg850 values. As stated in Munday and Washington (2017), this is indicative of the dry convection processes that are at play during the beginning of the rainy season over the region. Moving towards DJF, the high theta850 values move southwards, indicating that in the core of the rainy season, convection over the greater Angola region is not thermally induced, but there is a rather dynamical large-scale driver. In Fig. S3 the scatterplots between zg850 (x axis) and theta850 (y axis) for each month of the rainy season are shown, over all of southern Africa (land pixels only). The same plot, but with pixels only from the greater Angola region (14 to 25° E and from 11 to 19° S), is displayed in Fig. S4. Although the relationship between the two variables is not linear, they display a considerable association, especially over the greater Angola region.

In Howard and Washington (2018) AL events are identified using daily relative vorticity (ζ) at 800 hPa. Since u and v wind components are not available at 800 hPa (but at 850 hPa) for the CORDEX ensembles, we investigate whether the 850 hPa pressure level can be used instead. We also examine whether the ζ threshold has to be adjusted. In Howard and Washington (2018), AL events are identified within the region ranging from 14 to 25° E and from 11 to 19° S for mean daily ζ values $< -4 \times 10^{-5}\ \mathrm{s}^{-1}$. An additional issue that we take into account is that u and v wind components are not available on a daily time step for CMIP6, but only on a monthly time step. Hence, for consis-

tency reasons we work with monthly files in all ensembles (both CMIP, CORDEX) and in ERA5.

With regards to the question of whether the 850 hPa pressure level can be used instead of 800 hPa, we examine monthly relative vorticity in ERA5 in both pressure levels, within the region from 14 to 25° E and from 11 to 19° S (Fig. S5). Both distributions are very similar in shape, maxima and spread, although the distribution of ζ values at 800 hPa appear to have a shorter tail. On both panels, both the Howard and Washington (2018) and the Desbiolles et al. (2020) thresholds are indicated. We conclude that the 850 hPa pressure level can be used instead of 800 hPa. With regards to the fact that u and v wind components are available only on a monthly time step in CMIP6, we compare the daily and monthly relative vorticity values at 800 hPa in ERA5 for all the months of the rainy season (October–March) (Fig. S6). The difference in the y axis results from the fact that when ζ is calculated using a daily time step, the histogram is drawn using 5 421 825 values, while when the ζ is calculated using monthly u and v values, it is drawn using 178 200 values (for the period 1986–2005). As shown, the distribution of the monthly values has a much shorter tail and the Howard and Washington (2018) threshold appears to be very strict, as a criterion for the identification of AL events.

Concerning the question of what the optimal threshold for the identification of AL events in all datasets is, we investigate the statistical distribution of mean monthly cyclonic vorticities in all ensembles used, for the 850 hPa pressure level (Fig. S7). We conclude that the threshold used in Desbiolles et al. (2020) (ζ values $< -1.5 \times 10^{-5}\,\mathrm{s}^{-1}$) is reasonable, considering the shape of the distributions examined. However, when the Desbiolles et al. (2020) threshold is applied to the data, it is also found to be too strict, especially for CMIP5/6. Hence, we identify AL events having $\zeta < -0.00001\,\mathrm{s}^{-1}$. Lastly, we use geopotential height at 850 hPa for visual inspection only in ERA5 and CMIP5/6 ensembles.Lastly, the Theil–Sen slope (Theil, 1992; Sen, 1968) for monthly precipitation during the period 1986–2005 is calculated for each dataset. This is a non-parametric approach to estimate trends that is insensitive to outliers. Statistical significance is assessed using the Mann–Kendall test (Mann, 1945; Kendall, 1948).

3 Results

3.1 Climatology

Figure 1 displays monthly precipitation climatologies during October–March (rainy season over the study region) for ERA5 and for the ensemble means of seven additional types of datasets. At the beginning of the rainy season (October) all products display precipitation maxima at the northwestern part of the study region. Another precipitation maximum is observed in eastern South Africa. For both regions, there is a slight tendency for gauge-based products to yield approximately $1\,\mathrm{mm\,d}^{-1}$ less precipitation than reanalysis and satellite products. The CMIP5, CMIP6, CORDEX0.44 and CORDEX0.22 ensembles are also in agreement with regards to the location and amounts; however, CORDEX0.44 displays approximately $2\,\mathrm{mm\,d}^{-1}$ more precipitation over Angola. During November, the rainband extends southwards, and the region over South Africa experiencing high precipitation enlarges.

Moving towards the core of the rainy season (DJF) the precipitation maxima extends southwards following the collapse of the Congo air boundary (CAB) (Howard and Washington, 2019), and high precipitation amounts are also observed over the eastern part of the study region. More specifically during January, high precipitation amounts ($> 10\,\mathrm{mm\,d}^{-1}$) are observed over an extended region in northern Mozambique for non-merging satellite products (Satellite-NoMerge). This area is also identified as a region of high precipitation in gauge-based products and in merging satellite products, however, with a smaller magnitude. In ERA5, the spatial pattern of precipitation is more patchy and exhibits precipitation amounts higher than observed in the wider region of Lake Malawi, reaching extremely high values ($34\,\mathrm{mm\,d}^{-1}$), as also indicated in the known precipitation issues of ERA5 over Africa (Hersbach et al., 2020). During DJF both CORDEX0.44 and CORDEX0.22 ensembles display precipitation values $> 3\,\mathrm{mm\,d}^{-1}$ over almost all of the SAF region. This observation is also consistent in CMIP5 and CMIP6; however, maximum precipitation amounts in CMIP5 and CMIP6 are approximately $> 3\,\mathrm{mm\,d}^{-1}$ larger than in the CORDEX ensembles. It is noteworthy that in CORDEX0.22 during DJF, there are parts over northern SAF experiencing precipitation amounts $> 10\,\mathrm{mm\,d}^{-1}$, a feature that is not seen in any of the observational products. After investigating the individual ensemble members used in the CORDEX0.22 ensemble (Fig. S8), we see that the excess amount of precipitation is removed from the CORDEX0.22 ensemble mean when RegCM4-7 simulations are not included (Fig. S9). In March, the rainband starts its northward shift; nevertheless, high precipitation amounts are still observed over the eastern parts of the study region and over the coastal region of Angola. The retreat of the rainband is evident in both CORDEX0.44 and CORDEX0.22; however, CMIP5 and CMIP6 still exhibit extended regions of high precipitation.

In Fig. 2, SD values for the 7 ensembles are presented during the months October–March for the period 1986–2005 expressed as millimeters per day ($\mathrm{mm\,d}^{-1}$). SD is used as a measure of the within-ensemble agreement. As shown for gauge-based products, during October and November high SD values are observed primarily over Angola. For the months December–March Angola remains a high-SD region; however, increased SD values are also observed over the eastern parts of SAF and especially over northern Mozambique. An important aspect influencing gauge-based products is the

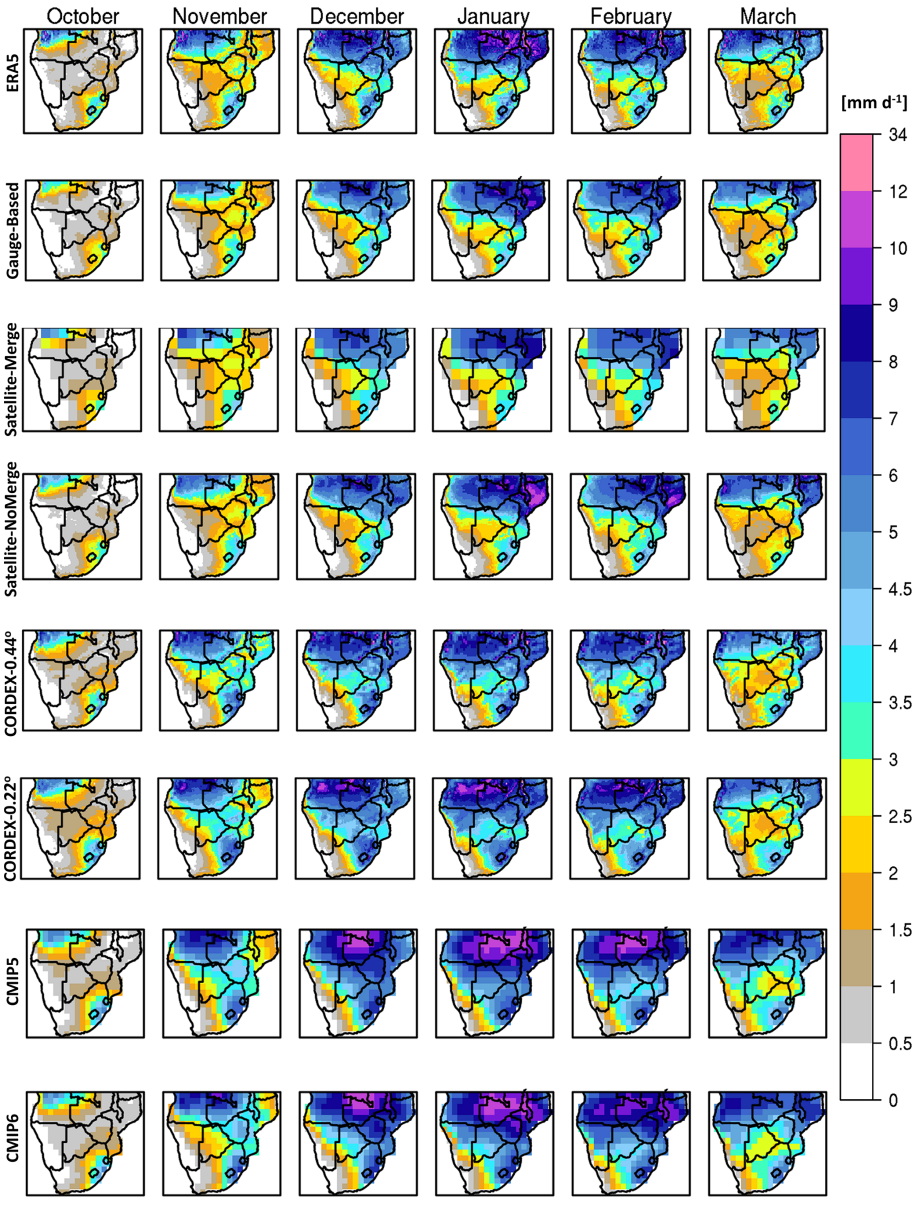

Figure 1. Monthly precipitation climatologies during the period 1986–2005 in mm d^{-1}. More specifically, from top to bottom – ERA5 reanalysis dataset; Gauge-based: ensemble mean of datasets that were produced by employing spatial interpolation methods using rain gauges/station data; Satellite-Merge: ensemble mean of all satellite products that merge with rain gauges/station data; Satellite-NoMerge: ensemble mean of satellite products that do not merge with rain gauges/station data; CORDEX-0.44°: ensemble mean of regional climate model simulations performed in the context of the Coordinated Regional Climate Downscaling Experiment (CORDEX) – Africa domain with a spatial resolution equal to 0.44° × 0.44°; CORDEX-0.22°: CORDEX-Africa simulations with a spatial resolution equal to 0.22° × 0.22°; CMIP5: ensemble mean of general circulation models participating in the Coupled Model Intercomparison Project Phase 5 (CMIP5) that were used as forcing in the CORDEX-Africa simulations; CMIP6: ensemble mean of general circulation models participating in the Coupled Model Intercomparison Project Phase 6.

spatiotemporal coverage of the rain gauges used (Le Coz and van de Giesen, 2020), which is highly variable between regions and reporting periods. More specifically, after the 1970s the rain gauge coverage over Africa has decreased significantly (Janowiak, 1988), and the gauge network has been particularly sparse over the SAF region (Lorenz and Kunstmann, 2012; Giesen et al., 2014), which further implies that gauge-based products depend on extrapolating values from surrounding gauges. Therefore, station density and the interpolation method employed are key factors in determining the accuracy of the final product (Le Coz and van de Giesen, 2020). The high SD values over Angola are mainly due to

the scarcity of available rain gauges used in the interpolation method (Fig. S10). After 1995, there is a noticeable reduction of the station and rain gauge data used over the SAF region (Fig. S11) for three of the gauge-based products.

A similar spatiotemporal pattern of SD is also observed in satellite-based products (Sat-Merge) which employ algorithms that merge rain gauges with thermal-infrared (TIR) images. This is indicative of the strong impact that the location and number of rain gauges exert on satellite algorithms that employ merging techniques (Maidment et al., 2014, 2015). The spatiotemporal pattern of SD for satellite-based products that do not merge with gauges (Sat-NoMerge) displays low SD values for October and November; however, during DJF localized areas of high SD appear over Angola, Zambia, Malawi and Mozambique. The satellite products used in this ensemble are based on TIR images, and precipitation is indirectly assessed through cloud top temperature (Tarnavsky et al., 2014; Ashouri et al., 2015; Funk et al., 2015). Hence, the occurrence and severity of precipitation is calculated based on a temperature threshold. In cases that the threshold is set to very low cloud top temperature values, the algorithm has high skill at identifying deep convection; however, warm rain events are not adequately captured (Toté et al., 2015). As shown in Fig. 2, high SD values in non-merging satellite products are primarily observed over coastal regions and over regions where the elevation increases rapidly. These type of regions can be associated with orographic or frontal lifting of air masses (Houze, 2012), resulting in precipitation, without the threshold temperature of the cloud top being reached.

In the CORDEX0.44 ensemble SD values are $> 0.8\,\mathrm{mm\,d^{-1}}$ over almost all of the SAF region; however, very high SD values (3–9.8 $\mathrm{mm\,d^{-1}}$) are observed in the coastal part of Angola and over the Lake Malawi region during November–March. SD values in CORDEX0.22 are considerably larger throughout the greater part of SAF, especially during DJF. In the CMIP5 ensemble the spatiotemporal pattern of SD values exceeds $2\,\mathrm{mm\,d^{-1}}$ during November–March throughout the whole SAF region. CMIP6 displays a similar SD pattern. During March, however, CMIP6 displays a substantial improvement in the agreement between its ensemble members. Overall, for the whole extent of SAF, the CORDEX-Africa ensembles display greater agreement among ensemble members, however SD values become large over specific localized regions, mainly in western Angola and in the Malawi region. The CMIP5 and CMIP6 ensembles, although not displaying the localized extreme SD values as CORDEX-Africa, display generally high SD values throughout the whole extent of SAF.

3.2 Annual cycle

Figure 3 displays the annual cycle of precipitation in the CORDEX0.44, CORDEX0.22, CMIP5, CMIP6 and observational ensembles for land grid points. All datasets capture the unimodal distribution of precipitation over SAF; however, considerable differences in precipitation amount and spread are observed.

Specifically, the CMIP5 ensemble exhibits significantly higher precipitation amounts than both CORDEX and observational ensembles. This difference becomes particularly pronounced during the rainy season, with CMIP5 yielding approximately $2\,\mathrm{mm\,d^{-1}}$ more precipitation than the observational ensemble. It is also notable that for November–February, even the driest ensemble members of CMIP5 yield approximately $1\,\mathrm{mm\,d^{-1}}$ more precipitation than the wettest ensemble members of the observational data. This is in agreement with Munday and Washington (2018), who identified a systematic wet bias over SAF in CMIP5 that was associated with an intensified northeasterly transport of moisture that erroneously reaches SAF, due to the poorly represented orography in the region of Tanzania and Malawi (which would hinder moisture originating from the Indian ocean from reaching SAF and instead force it to recurve towards the region of Madagascar). The behavior of CMIP6 is similar to CMIP5, with a slightly smaller ensemble spread during January–March and a considerable reduction in spread during November.

The CORDEX0.44 ensemble reduces precipitation amounts during the core of the rainy season (DJF) compared to CMIP5; however, its behavior during the rest of the months is complicated. More specifically, during August–October CORDEX0.44 displays slightly higher precipitation amounts compared to CMIP5. During November, the difference between the CORDEX0.44 and the CMIP5 ensembles becomes noticeable, with the CMIP5 ensemble mean becoming $0.4\,\mathrm{mm\,d^{-1}}$ larger than the CORDEX0.44 ensemble mean. During DJF the differences between the two ensembles maximize, with the CORDEX0.44 ensemble displaying good agreement with the OBS ensemble ($< 1\,\mathrm{mm\,d^{-1}}$ difference in the ensemble means of CORDEX0.44 and OBS). From March until July, the difference between the CORDEX0.44 and CMIP5 ensembles starts to reduce gradually. The ensemble mean of the CORDEX0.22 ensemble is similar to that of the CORDEX0.44 ensemble; however, its spread during the rainy season is considerably larger. Taking into consideration that excess precipitation in the CORDEX0.22 ensemble is introduced by RegCM4-7, we observe that the ensemble spread of the CORDEX0.22 ensemble is reduced, when RegCM4-7 is not included in the CORDEX0.22 ensemble (Fig. S12).

Since the maximum impact of the northeasterly moisture transport into SAF responsible for the wet bias in CMIP5 occurs during DJF (Munday and Washington, 2018), the impact of the CORDEX0.44 and CORDEX0.22 increase in resolution and the effect of the improved representation of topography is also more intensely identified during DJF. As displayed in Fig. 4, surface orography is substantially improved in the CORDEX ensembles, relative to CMIP5/6. The

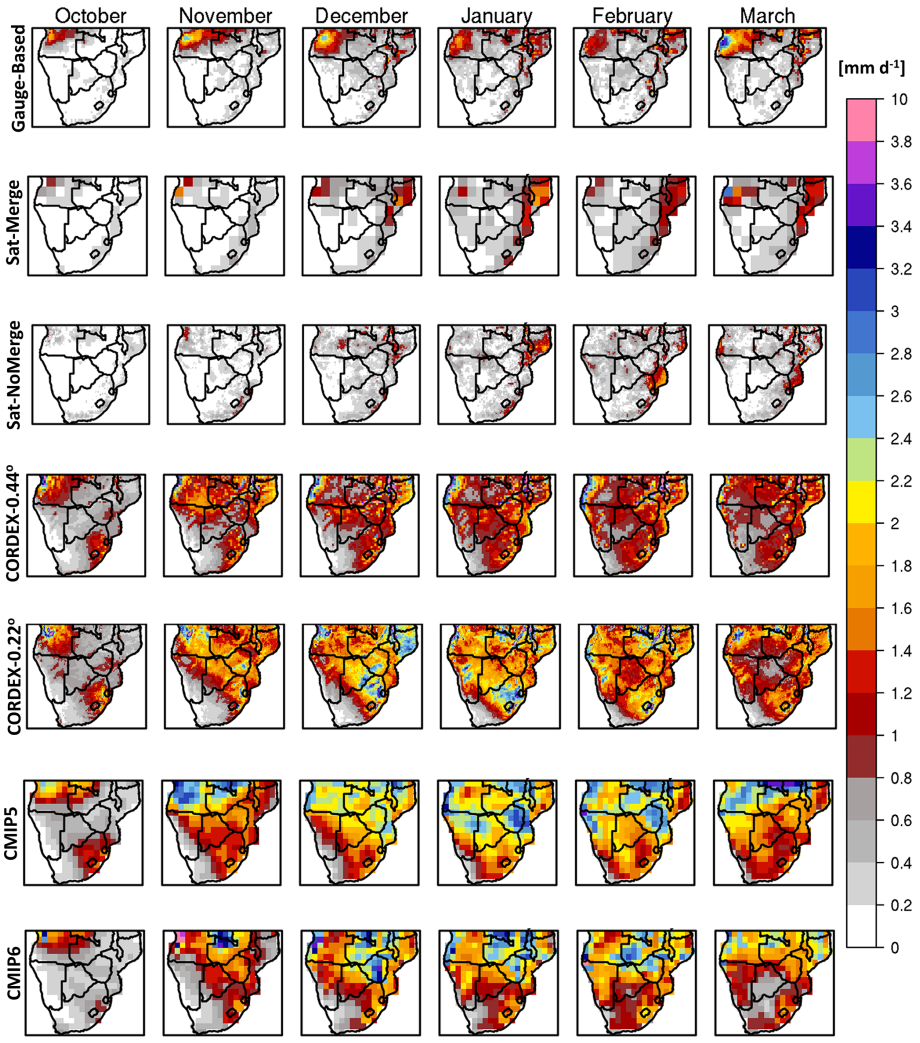

Figure 2. Standard deviation of monthly precipitation [mm d^{-1}] during the period 1986–2005. Rows indicate the ensemble means analyzed. From top to bottom – Gauge-based: ensemble mean of datasets that were produced by employing spatial interpolation methods using rain gauges/station data; Sat-Merge: ensemble mean of all satellite products that merge with rain gauges/station data; Sat-NoMerge: ensemble mean of satellite products that do not merge with rain gauges/station data; CORDEX-0.44°: ensemble mean of regional climate model simulations performed in the context of the Coordinated Regional Climate Downscaling Experiment – Africa domain with a spatial resolution equal to 0.44° × 0.44°; CORDEX-0.22°: CORDEX-Africa simulations with a spatial resolution equal to 0.22° × 0.22°; CMIP5: ensemble mean of general circulation models participating in the Coupled Model Intercomparison Project Phase 5 (CMIP5) that were used as forcing in the CORDEX-Africa simulations; CMIP6: ensemble mean of general circulation models participating in the Coupled Model Intercomparison Project Phase 6.

improvement of orography has a further effect in blocking moisture transport entering SAF from the northeast, especially during December–January, as seen in Fig. 5.

3.3 Angola low

In Fig. 6 the mean monthly climatology of the AL pressure system during the rainy season is displayed for the period 1986–2005. The AL is explored by means of relative vorticity, only within the region extending from 14 to 25° E and from 11 to 19° S. This region is characterized by Howard and Washington (2018) as the main region of interest for the AL. The relative vorticity for $\zeta < -0.00001\,s^{-1}$ over the whole SAF is shown in Fig. S13. In addition, potential temperature at 850 hPa (theta850) is overlaid on relative vorticity, with the first contour set at 308 K, the last contour set at 318 K and the increment between the isotherms being set to 2 K. For ERA5 and the ensemble means of CMIP5/6 the geopotential height at 850 hPa was also available.

As shown in Fig. 6, ζ values for October are greater than $> -0.000025\,s^{-1}$ for ERA5 and CORDEX0.44/0.22 and are relatively weaker in CMIP5 and even weaker in CMIP6. The high cyclonic vorticity values overlap with the

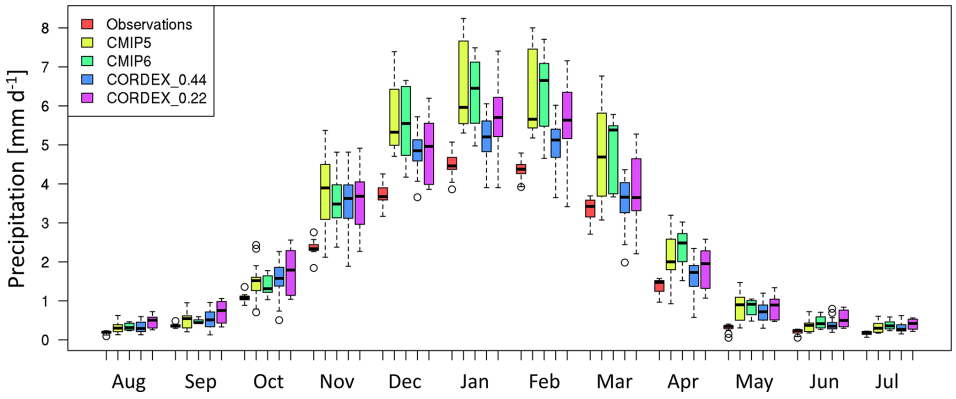

Figure 3. Annual cycle of monthly precipitation during 1986–2005 for the ensemble of observational data (gauge-based, satellite and reanalysis), CMIP5 (Coupled Model Intercomparison Project Phase 5), CMIP6 (Coupled Model Intercomparison Project Phase 6), CORDEX0.44 (Coordinated Regional Climate Downscaling Experiment – Africa domain with a spatial resolution equal to 0.44° × 0.44°) and CORDEX-0.22° (CORDEX-Africa simulations with a spatial resolution equal to 0.22° × 0.22°). The thick horizontal black lines indicate the ensemble median for each month, the box encloses the interquartile range and the tails denote the full ensemble range. Circles represent the outliers for each ensemble. Only grid points are considered.

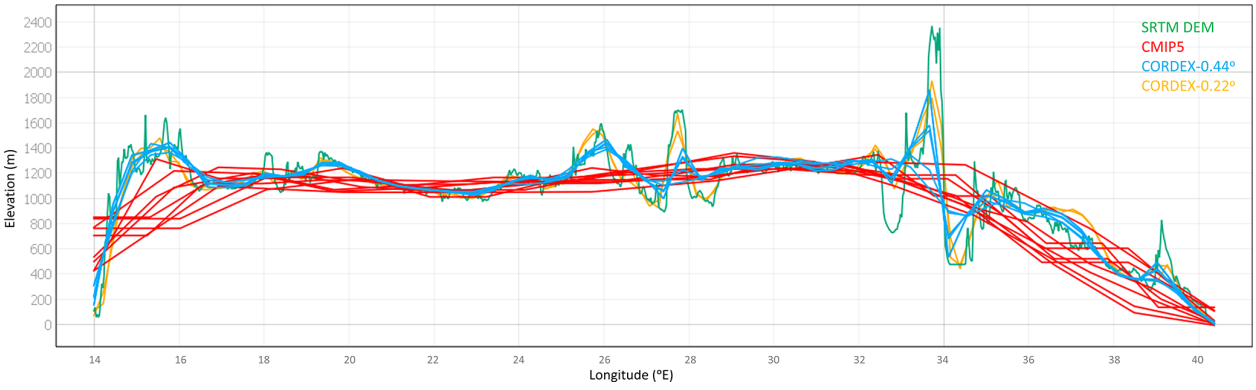

Figure 4. Cross section of surface elevation at 11° S across southern Africa for the Shuttle Radar Topography Mission (SRTM) digital elevation model (in green), the surface altitude as represented in the CMIP5 (Coupled Model Intercomparison Project Phase 5) global climate models (in red), the surface altitude as represented in the CORDEX0.44 (Coordinated Regional Climate Downscaling Experiment – Africa domain with a spatial resolution equal to 0.44° × 0.44°) (in blue) and the surface altitude as represented in the CORDEX-0.22° (CORDEX-Africa simulations with a spatial resolution equal to 0.22° × 0.22°) (in yellow).

312 K isotherm for all datasets. We also observe that the isoheights in the ERA5 and CMIP5/6 ensembles are closely collocated with the 312 K isotherms, indicating that the low pressure system observed over the region is caused by the excess heating of the air, and hence it is indicative of a typical low-pressure heat system (Munday and Washington, 2017; Howard and Washington, 2018). Moving to November, the picture is similar; however, the isotherms display a southward extension, while the 850 hPa isoheights deepen by ∼ 5 m in ERA5 and CMIP5/6. In December, all datasets display an increase in cyclonic vorticity; however, the maximum heating area has migrated southwards over the Kalahari region. This fact indicates that cyclonic activity over the AL region is no longer due to thermal causes. During December and January the cyclonic activity is enhanced in all datasets and the isotherms have migrated even more southwards, forming the Kalahari heat low, which is distinct from the AL. We also observe that during January, the isoheights in ERA5 and CMIP5/6 become even deeper. We also note that the elongated trough during December–January can be indicative of the formation of TTTs, which account for a large proportion of rainfall over SAF (Hart et al., 2010). February displays similar spatial patterns to January for all datasets, albeit slightly weakened for all variables. In March, cyclonic activity over the region has seized. Taking into consideration the distribution of the cyclonic vorticity field, we observe that in higher-resolution datasets (ERA5, CORDEX0.22) high vorticity values are more severe, in very localized regions. With respect to potential temperature, we observe for October and November all datasets having a similar distribution

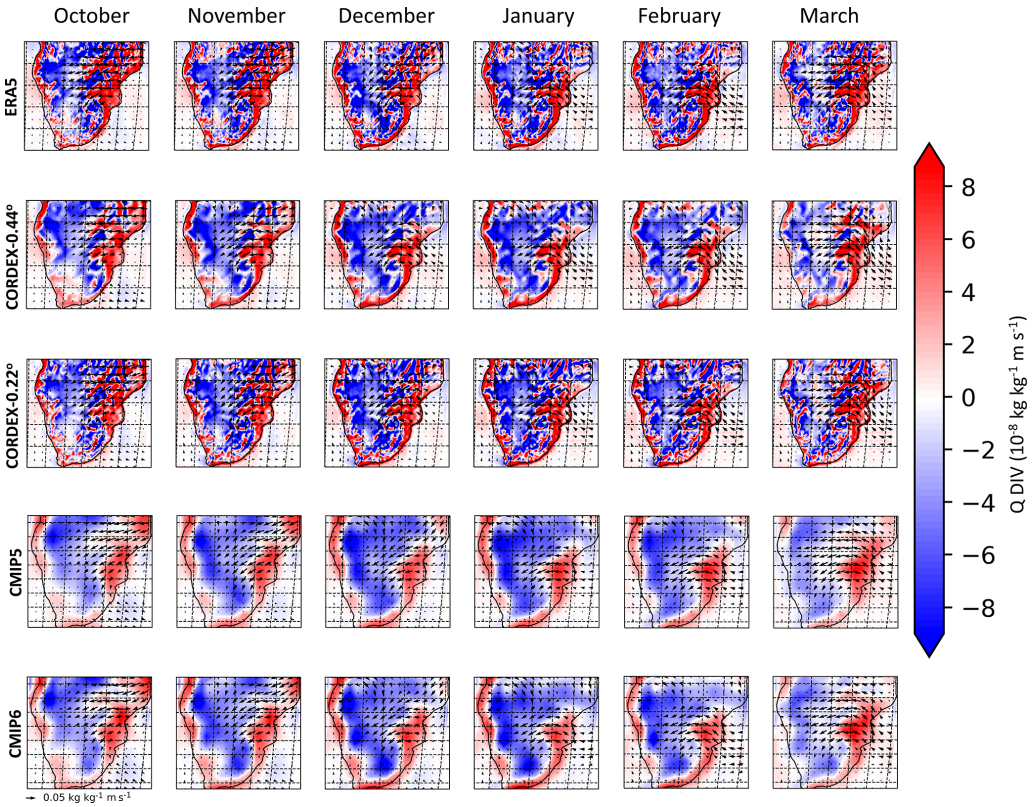

Figure 5. Mean monthly moisture flux and divergence at 850 hPa during the period 1986–2005. Rows indicate the ensemble means analyzed. From top to bottom: ERA5, ensemble mean of CORDEX0.44°, CORDEX0.22°, CMIP5 and CMIP6 simulations.

of theta850 values. We also note that CMIP6, in general, displays higher theta850 values and lower geopotential heights, relative to CMIP5.

3.4 Precipitation indices

Total annual precipitation (PRCPTOT) is displayed in Fig. 7a. The mean of the CMIP6 ensemble displays the largest amounts of PRCPTOT (approximately 1000 mm yr^{-1}), with CMIP5 following closely. The CORDEX0.44 and CORDEX0.22 ensembles display a very similar behavior, systematically reducing PRCPTOT amounts seen in CMIP5/6 by approximately 200 mm yr^{-1}, yielding PRCPTOT values closer to that of the observational datasets. Both CMIP5/6 and CORDEX0.22/0.44 ensembles display similar within-ensemble variability. The ensemble mean of the observational datasets is considerably lower than CORDEX ensembles and displays an interannual variability between 500–800 mm yr^{-1}. The ensemble means of both CMIP5/6 and CORDEX0.44/0.22 fail to reproduce the interannual variability of the observational ensemble. In Fig. 7b the annual maximum 1 d precipitation (Rx1Day) is displayed. For Rx1Day, the mean of the CMIP5 ensemble is in close agreement with the mean of the observational ensemble (approximately 40 mm d^{-1}). The ensemble mean of CORDEX0.44 yields larger precipitation amounts (approximately 55 mm d^{-1}) than CMIP5 and the observational ensemble. The CORDEX0.22 ensemble mean displays even higher values (approximately 75 mm d^{-1}). As shown in Fig. 7b, the CORDEX0.44 ensemble mean is influenced by higher Rx1Day values, originating from ensemble members that cluster within the range 65–85 mm d^{-1}. The spread of the CMIP5 ensemble is comparable to that of the observational data; however, the CORDEX0.44/0.22 ensemble spreads are still larger, ranging from 25–85 and from 55–100 mm d^{-1}, respectively. The CMIP6 ensemble falls between the CORDEX0.44 and CMIP5 ensembles, with a spread comparable to that of CMIP5. In Fig. 7c the annual number of days with daily precipitation greater than 10 mm (R10mm) is presented. It is noted that the ensemble mean of the CORDEX0.44 ensemble is close to that of the observational datasets ($\sim$ 25 d yr^{-1} with daily precipitation greater than 10 mm), while the ensemble mean of CORDEX0.22 almost coincides with the mean of the observational datasets. The mean of the CMIP5 ensemble yields approximately 34 d of extreme precipitation annually. It is also highlighted that the CMIP5 ensemble displays a large range of R10mm values (10–55 d yr^{-1}). Again, the CMIP6 ensemble mean coincides with that of CMIP5. In Fig. 7d the annual number of days with daily precipitation

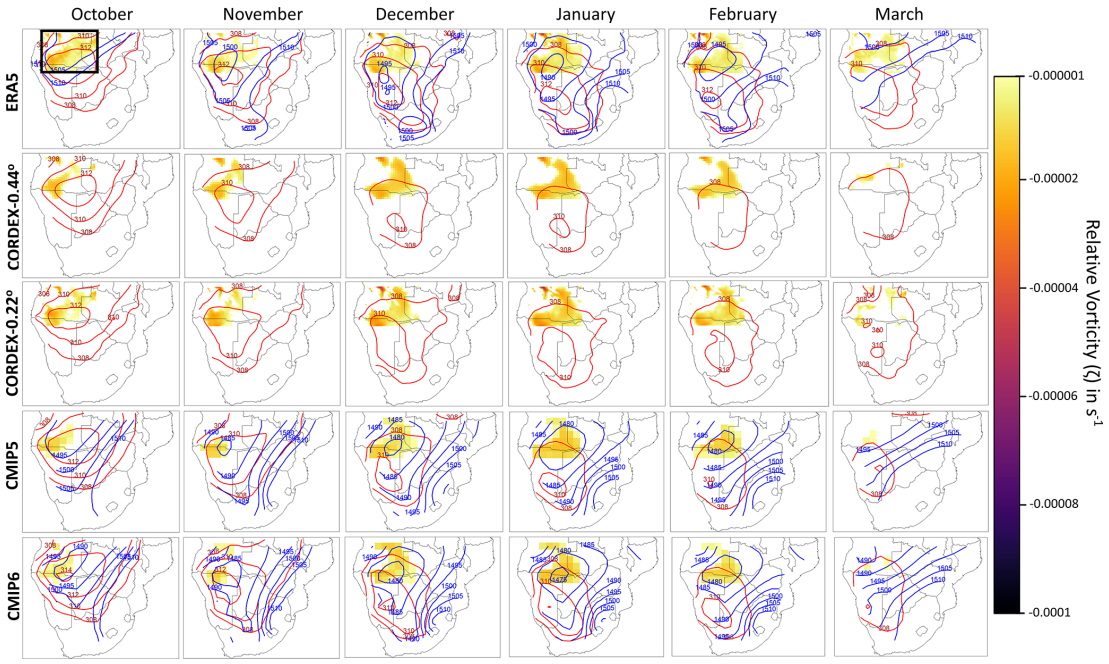

Figure 6. Monthly climatologies of the Angola Low pressure system during the rainy season for the period 1986–2005. Filled contours indicate cyclonic relative vorticity (ζ) for $\zeta < -0.00001\,s^{-1}$ over the region extending from 14 to 25° E and from 11 to 19° S. Red lines indicate the isotherms of potential temperature at 850 hPa, having an increment of 2 K. Blue lines indicate isoheights of the geopotential height at 850 hPa, having an increment of 5 m. CORDEX0.44 and CORDEX0.22 are not plotted with geopotential isoheights, because this variable was not available for CORDEX simulations. From top to bottom: ERA5, ensemble mean of CORDEX0.44°, CORDEX0.22°, CMIP5 and CMIP6 simulations. Black box indicates the region from 14 to 25° E and from 11 to 19° S.

greater than 20 mm (R20mm) is shown. There is close agreement between the CMIP5 and CORDEX0.44 ensembles; however, both datasets overestimate R20mm relative to the observational data. Again, the CMIP5 ensemble displays the largest spread, and a very weak interannual variability is seen on both CMIP5 and CORDEX0.44 ensemble means. The CMIP6 ensemble mean is slightly larger than its predecessor. R20mm in CORDEX0.22 mean is almost identical to the mean of the CMIP6 ensemble.

3.5 Trends

In Fig. 8 the monthly precipitation trends for the rainy season of the period 1986–2005 are displayed for all three observational data (gauge-based, SatelliteMerge, Satellite-NoMerge) and for the CORDEX0.44, CORDEX0.22, CMIP5 and CMIP6 ensembles. Precipitation trends display considerable agreement among all three observational datasets, concerning both the signal and the magnitude of the trend. However, the CORDEX0.44/0.22 and CMIP5/6 ensembles display trends that are considerably smaller in magnitude. In addition, CORDEX0.44, CMIP5 and CMIP6 ensembles display fairly distinct spatial patterns that are not in agreement either among themselves or with the spatial pattern of precipitation trends displayed by the observational datasets. In general, we observe that the signal between CORDEX0.44 and CORDEX0.22 is consistent, with trends in CORDEX0.22 displaying a larger magnitude.

More specifically, during October, all observational products display decreasing trends for most of SAF that reach up to $-0.1\,mm\,d^{-1}$ per 20 years. During November the signal changes and SAF experiences increasing trends, with an exception for NW SAF, northern Mozambique and regions of eastern South Africa. During December increasing trends become even more spatially extended and pronounced, especially for satellite products. During January, certain areas of decreasing trends over northern SAF appear, while during February decreasing trends are observed over almost the whole extent of SAF. In March, increasing trends are observed in the region extending from southern Mozambique and stretching towards Zimbabwe and southern Zambia.

Monthly precipitation trends in the CORDEX0.44 ensemble are significantly weaker than in the observational datasets and display a precipitation increase during October–December. After January certain regions of intensified decreasing trends appear over southern Angola–northern Namibia and Botswana (January) and over Botswana and South Africa (February). The pattern of trends is relatively similar in CORDEX0.22; however, the trend magnitude is more enhanced. In CMIP5 decreasing trends are observed during October, but for November increasing trends are observed over the northern part of SAF. During December,

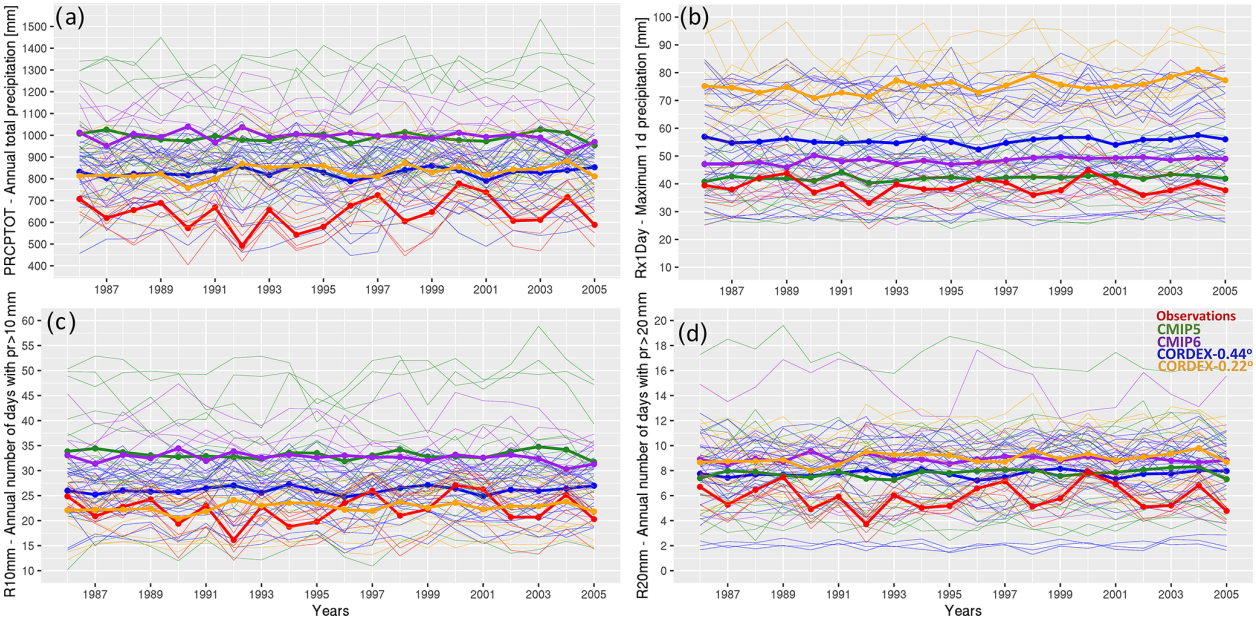

Figure 7. Time series of the ETCCDI indices over southern Africa (10 to 42° E and 10 to 35° S) for the observational ensemble in red (gauge-based, satellite and reanalysis), CMIP5 (Coupled Model Intercomparison Project Phase 5) ensemble in green, CMIP6 (Coupled Model Intercomparison Project Phase 6) ensemble in purple, CORDEX-0.44° ensemble mean of regional climate model simulations performed in the context of the Coordinated Regional Climate Downscaling Experiment – Africa domain with a spatial resolution equal to 0.44° × 0.44° in blue and CORDEX-0.22° in orange. Thin lines display single ensemble members, thick lines display ensemble means. The *y* axis on each panel depicts **(a)** PRCPTOT (total annual precipitation), **(b)** Rx1Day (annual maximum daily precipitation), **(c)** R10mm (annual number of days with daily precipitation > 10 mm) and **(d)** R20mm (annual number of days with daily precipitation > 20 mm).

strong increasing trends (0.1 mm d^{-1} per 20 years) appear for central SAF, while during January almost all of the SAF region (with an exception for Mozambique) experiences decreasing precipitation trends. In CMIP6 persistent drying trends are observed almost throughout the whole of SAF and are particularly strong during January–February (−0.1 mm d^{-1} per 20 years). During March, however, the signal is reversed. Statistical significance assessed with the Mann–Kendall test is shown in Fig. S14. The number of ensemble members displaying increasing or decreasing trends in each ensemble is shown in Fig. S15.

4 Discussion and conclusions

The analysis of the SD among the different observational products highlights the fact that precipitation assessment requires consultation of multiple (gauge-based, satellite and reanalysis) products. If this is not possible, then it is highly recommended that the spatial distribution and frequency of reporting of the underlying station data are examined, for each respective precipitation product in use. This should also be regarded in cases when gauge-based or satellite products are utilized for model evaluation purposes. Moreover, satellite products that merge with rain gauges should not be considered independent from gauge-based products that exploit similar gauge networks. In addition, we note that SD in the CORDEX0.44 ensemble is considerably lower than in the CMIP5/6 ensembles, supplying evidence that the CORDEX0.44 set of simulations provide more constrained results and can thus be considered to be a suitable dataset for climate impact assessment studies over SAF. However, that is not entirely the case for the CORDEX0.22 ensemble, which, although it displays SD values smaller to that of CMIP5/6, still yields SD values higher than that of CORDEX0.44.

Concerning the annual cycle of precipitation, we note that although the seasonality is captured reasonably by both the CMIP and CORDEX-Africa ensembles, still, there are considerable differences between them. More specifically, we conclude that the CORDEX0.44 ensemble exhibits smaller ensemble spread for all months of the rainy season compared to the driving GCMs (CMIP5). We also conclude that the strong wet bias over SAF in the CMIP5 ensemble (Munday and Washington, 2018) is considerably reduced in the CORDEX0.44 ensemble. This bias is still evident in CMIP6. A plethora of references in the literature (Reason and Jagadheesha, 2005; Lyon and Mason, 2007; Crétat et al., 2019; Munday and Washington, 2017; Howard and Washington, 2018) have highlighted the importance of the AL pressure system in modulating precipitation over SAF. We note that the strength of the AL as assessed in the current study was simulated to be weaker in the CORDEX0.44 than in the CORDEX0.22 ensemble. This may partly explain why pre-

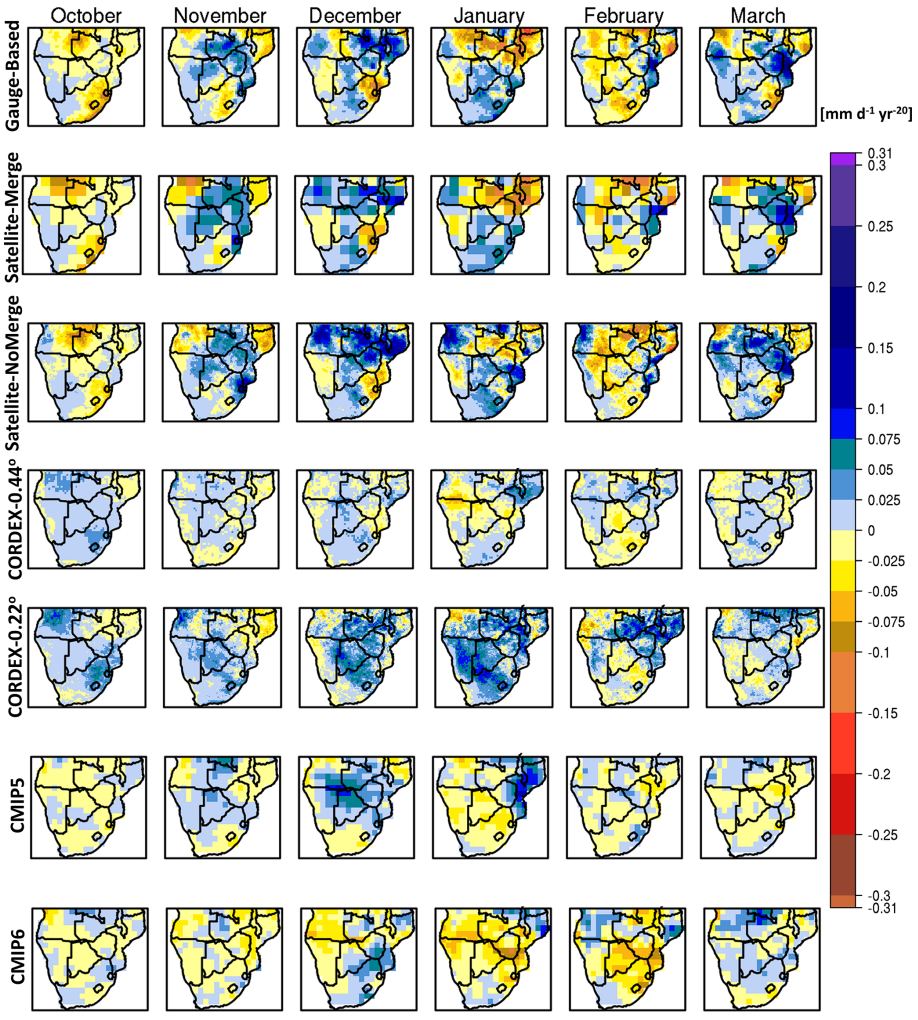

Figure 8. Trends for monthly precipitation for the period 1986–2005 [mm d^{-1} per 20 years] calculated using Sen's slope. Rows indicate the ensemble mean of trends produced by each ensemble member. From top to bottom – Gauge-Based: ensemble mean of datasets that were produced by employing spatial interpolation methods using rain gauges/station data. Satellite-Merge: ensemble mean of all satellite products that merge with rain gauges/station data. Satellite-NoMerge: ensemble mean of satellite products that do not merge with rain gauges/station data. CORDEX-0.44°: ensemble mean of regional climate model simulations performed in the context of the Coordinated Regional Climate Downscaling Experiment – Africa domain with a spatial resolution equal to 0.44° × 0.44°. CORDEX-0.22°: CORDEX-Africa simulations with a spatial resolution equal to 0.22° × 0.22°. CMIP5: ensemble mean of general circulation models participating in the Coupled Model Intercomparison Project Phase 5 (CMIP5) that were used as forcing in the CORDEX-0.44° simulations. CMIP6: ensemble mean of general circulation models participating in the Coupled Model Intercomparison Project Phase 6.

cipitation in the CORDEX0.44 ensemble is reduced, relative to the CORDEX0.22 ensemble. However, there is need for a more in-depth dynamical analysis of the simulation of the AL in the CORDEX-Africa ensemble (both CORDEX0.44 and CORDEX0.22) and its impact on modulating precipitation seasonality and patterns over SAF.

The use of the four ETCCDI indices demonstrated that the CORDEX-Africa ensemble yields results that are in closer agreement to the observational data, compared to CMIP5/6 ensembles. It is, nevertheless, noticeable that the improvement in the CORDEX-Africa ensemble is most evident when the ensemble mean is used. This highlights the fact that the ensemble mean performance is improved, relative to the performance of individual models (Nikulin et al., 2012). For this reason, it is advisable that climate impact studies employ multi-model ensemble means, as a method of obtaining the consensus climatic information emanating from various models (Duan et al., 2019). In addition, we underline the fact that in all indices the ensemble means of CMIP5/6 and CORDEX-Africa were not able to reproduce the interannual variability that was seen in the observational ensemble. This remark is in agreement with the fact that the task of reproducing precipitation variability across various timescales using the CMIP5 ensemble is known to present

challenges (Dieppois et al., 2019), which inevitably cascade into the CORDEX-Africa simulations that are forced with CMIP5 GCMs (Dosio et al., 2015). Lastly, even though the CORDEX-Africa ensembles reduce precipitation amounts over SAF, their use in drought-related impact studies should take into consideration that they still yield larger precipitation amounts than the observational data, which might eventually lead to underestimation of drought risk.

Precipitation trends during the rainy season displayed high spatial variability depending on the month. All observed (gauge-based and satellite) trends display substantial spatial agreement. The precipitation trends obtained by the CMIP5/6 and CORDEX0.44/0.22 ensembles did not display consistency with the trends obtained from the observational datasets. This is not entirely unexpected, due to the role of internal variability compared to external forcing in recent decades (Pierce et al., 2009), unlike temperature trends which have been shown to have a good agreement between the CORDEX-Africa (at 0.44° of spatial resolution) and CMIP5 ensembles with observed temperature trends (Dosio and Panitz, 2016; Warnatzsch and Reay, 2019). Nonetheless, we note that the trend signal between CORDEX0.44 and CORDEX0.22 is consistent, with CORDEX0.22 in general enhancing the CORDEX0.44 precipitation trends.

In conclusion, while CORDEX0.44 displays marked improvement over coarser-resolution products, there are still further improvements to be made. More specifically, since the wet bias in RCM simulations persists (although considerably reduced relative to GCMs), it is necessary that precipitation over southern Africa is no longer assessed based on bulk descriptive statistics, but that there will be a shift towards process-based evaluation, where the dynamical and thermodynamical characteristics of specific atmospheric features are investigated more thoroughly in the CORDEX-Africa simulations. For this reason, it is imperative that all institutes submitting RCM simulations in data repositories such as the Earth System Grid Federation or the Copernicus Climate Data Store provide model output data on multiple pressure levels, so that a fair comparison with the CMIP community would be possible. In addition, since the climate of southern Africa is highly coupled with the moisture transport coming from the adjacent oceans, it is necessary that the next generation of RCM simulations within CORDEX-Africa are performed coupled with ocean models. Lastly, since convection over southern Africa has a strong thermal component during specific months of the year (October–November), it is necessary that the land–atmosphere coupling processes within each RCM are examined in more detail, with coordinated efforts such as the LUCAS Flagship Pilot Study (https://ms.hereon.de/cordex_fps_lucas/index.php.en, last access: 1 November 2021), as performed in the Euro-CORDEX domain. In the world of regional climate modeling community, the 0.44° resolution of CORDEX-Africa is no longer state of the art, and ensemble efforts are now approaching convection-permitting grid spacing (i.e., < 4 km) in some parts of the world (Ban et al., 2021; Pichelli et al., 2021). We also note that increasing effort should be made with regards to understanding the improvements made from CORDEX0.44 simulations to CORDEX0.22. Although higher resolution is a desired target in the climate modeling community due to the more realistic representation of processes that it offers, still it should not be used as a panacea. In the current work we identified certain weaknesses in the CORDEX0.22 ensemble, that should be addressed before the community populates further its simulation matrix. The next generation ensembles for Africa will hopefully provide insight and improvements to the challenges described here.

Code and data availability. Analysis was performed using the R Project for Statistical Computing (https://www.r-project.org/, R Core Team, 2021), the Climate Data Operators (CDO) (https://code.mpimet.mpg.de/projects/cdo/, Schulzweida, 2021) and Bash programming routines. Processing scripts are available via ZENODO under the following DOI: https://doi.org/10.5281/zenodo.4725441 (Karypidou, 2021). CMIP5, CMIP6 and CORDEX-Africa daily precipitation data were retrieved from the Earth System Grid Federation (ESGF) portal (https://esgf-data.dkrz.de/projects/esgf-dkrz/, ESGF-DKRZ, 2021). CMIP5 temperature data at 850 hPa were retrieved from the Climate Data Store (CDS) (2021) (https://cds.climate.copernicus.eu/#!/home). CORDEX-Africa (both at 0.44 and 0.22° spatial resolution) temperature data at 850 hPa were retrieved from ESGF. Surface elevation data for CMIP5 and CORDEX-Africa were retrieved from ESGF. The Shuttle Radar Topography Mission (SRTM) digital elevation model was retrieved from https://srtm.csi.cgiar.org/ (last access: 21 June 2018, Farr et al., 2007). ERA5 data were retrieved from CDS. Climate Research Unit (CRU) data are available at https://crudata.uea.ac.uk/cru/data/hrg/ (last access: 22 April 2020, Harris et al., 2014). The University of Delaware (UDEL) data are available at https://psl.noaa.gov/data/gridded/data.UDel_AirT_Precip.html (last access: 14 May 2020, Willmott and Matsuura, 1995). The CPC Global Unified Gauge-Based Analysis of Daily Precipitation (CPC-Unified) was retrieved from https://psl.noaa.gov/data/gridded/data.cpc.globalprecip.html (last access: 18 April 2020, Chen et al., 2008). NOAA's PRECipitation REConstruction over Land dataset (PREC/L) was retrieved from https://psl.noaa.gov/data/gridded/data.precl.html (last access: 22 November 2019, Chen et al., 2002). The dataset of the Global Precipitation Climatology Centre (GPCC) was retrieved from https://psl.noaa.gov/data/gridded/data.gpcc.html (last access: 22 November 2020, Schneider et al., 2015). The Tropical Applications of Meteorology using SATellite (TAMSAT) data were retrieved from http://www.tamsat.org.uk/ (last access: 26 November 2020, Tarnavsky et al., 2014; Maidment et al., 2017). The Precipitation Estimation from Remotely Sensed Information using Artificial Neural Networks – Climate Data Record (PERSIANN-CDR) is available at https://chrsdata.eng.uci.edu/ (last access: 26 November 2020, Ashouri et al., 2015). The Climate Hazards Group InfraRed Precipitation with Station data (CHIRPS) products are available at https://www.chc.ucsb.edu/data/chirps

(last access: 20 May 2020, Funk et al., 2015). The CPC Merged Analysis of Precipitation (CMAP) dataset was retrieved from https://psl.noaa.gov/data/gridded/data.cmap.html (last access: 22 April 2020, Xie and Arkin, 1997). The Global Climatology Precipitation Project (GPCP) dataset was retrieved from https://psl.noaa.gov/data/gridded/data.gpcp.html (last access: 22 April 2020, Adler et al., 2012). The African Rainfall Climatology (ARC) dataset is available at https://iridl.ldeo.columbia.edu/SOURCES/.NOAA/.NCEP/.CPC/.FEWS/.Africa/.DAILY/.ARC2/.daily/index.html?Set-Language=en (last access: 25 April 2020, Novella and Thiaw, 2013).

Supplement. The supplement related to this article is available online at: https://doi.org/10.5194/gmd-15-3387-2022-supplement.

Author contributions. MCK, EK and SPS designed the research. MCK implemented the analysis and prepared the paper. EK and SPS edited the paper and provided corrections.

Competing interests. The contact author has declared that neither they nor their co-authors have any competing interests.

Disclaimer. Publisher's note: Copernicus Publications remains neutral with regard to jurisdictional claims in published maps and institutional affiliations.

Acknowledgements. Maria Chara Karypidou was funded by the Hellenic Foundation for Research & Innovation, under the second call for PhD candidates (application no. 1323). This article is funded by the AfriCultuReS project "Enhancing Food Security in African Agricultural Systems with the Support of Remote Sensing" (European Union's Horizon 2020 Research and Innovation Framework Programme under grant agreement no. 774652). The authors would like to thank the Scientific Support Centre of the Aristotle University of Thessaloniki (Greece) for providing computational and storage infrastructure and technical support.

This work is dedicated to the beautiful memory of Ms Anatoli Karypidou, "who lived faithfully a hidden life".

Financial support. This research has been supported by the Hellenic Foundation for Research & Innovation (H.F.R.I.) under the 2nd call for PhD Candidates (grant No. 1323).

Publication fees are covered by the Horizon 2020 AfriCultuReS project (grant no. 774652).

Review statement. This paper was edited by Augustin Colette and reviewed by two anonymous referees.

References

Adler, R. F., Gu, G., and Huffman, G. J.: Estimating Climatological Bias Errors for the Global Precipitation 118 Climatology Project (GPCP), J. Appl. Meteorol. Clim., 51, 84–99 https://doi.org/10.1175/JAMC-D-11-052.1, 2012.

African Development Bank Group (AFDBG): Southern Africa Economic Outlook 2019, African Development Bank, 2019.

Ashouri, H., Hsu, K.-L., Sorooshian, S., Braithwaite, D. K., Knapp, K. R., Cecil, L. D., Nelson, B. R., and Prat, O. P.: PERSIANN-CDR: Daily Precipitation Climate Data Record from Multisatellite Observations for Hydrological and Climate Studies, B. Am. Meteorol. Soc., 96, 69–83, https://doi.org/10.1175/BAMS-D-13-00068.1, 2015.

Azzarri, C. and Signorelli, S.: Climate and poverty in Africa South of the Sahara, World Dev., 125, 104691, https://doi.org/10.1016/j.worlddev.2019.104691, 2020.

Ban, N., Caillaud, C., Coppola, E., Pichelli, E., Sobolowski, S., Adinolfi, M., Ahrens, B., Alias, A., Anders, I., Bastin, S., Belusic, D., Berthou, S., Brisson, E., Cardoso, R. M., Chan, S., Christensen, O. B., Fernandez, J., Fita, L., Frisius, T., Gasparac, G., Giorgi, F., Goergen, K., Haugen, J. E., Hodnebrog, O., Kartsios, S., Katragkou, E., Kendon, E. J., Keuler, K., Lavin-Gullon, A., Lenderink, G., Leutwyler, D., Lorenz, T., Maraun, D., Mercogliano, P., Milovac, J., Panitz, H.-J., Raffa, M., Remedio, A. R., Schar, C., Soares, P. M. M., Srnec, L., Steensen, B. M., Stocchi, P., Tolle, M. H., Truhetz, H., Vergara-Temprado, J., de Vries, H., Warrach-Sagi, K., Wulfmeyer, V., and Zander, M.: The first multi-model ensemble of regional climate simulations at the kilometer-scale resolution, Part I: Evaluation of precipitation, Clim. Dynam., 57, 275–302, https://doi.org/10.1007/s00382-021-05708-w, 2021.

Chen, M., Shi, W., Xie, P., Silva, V. B. S., Kousky, V. E., Higgins, R. W., and Janowiak, J. E.: Assessing objective techniques for gauge-based analyses of global daily precipitation, J. Geophys. Res.-Atmos., 113, D04110, https://doi.org/10.1029/2007JD009132, 2008.

Chen, M., Xie, P., Janowiak, J. E., and Arkin, P. A.: Global Land Precipitation: A 50-yr Monthly Analysis Based on 136 Gauge Observations, J. Hydrometeorol., 3, 249–266, https://doi.org/10.1175/1525-7541(2002)003<0249:GLPAYM>2.0.CO;2, 2002.

Chinowsky, P. S., Schweikert, A. E., Strzepek, N. L., and Strzepek, K.: Infrastructure and climate change: a study of impacts and adaptations in Malawi, Mozambique, and Zambia, Climatic Change, 130, 49–62, https://doi.org/10.1007/s10584-014-1219-8, 2015.

Climate Data Store (CDS): https://cds.climate.copernicus.eu/#!/home, last access: 1 September 2021.

Coppola, E., Raffaele, F., Giorgi, F., Giuliani, G., Xuejie, G., Ciarlo, J. M., Sines, T. R., Torres-Alavez, J. A., Das, S., di Sante, F., Pichelli, E., Glazer, R., Müller, S. K., Abba Omar, S., Ashfaq, M., Bukovsky, M., Im, E.-S., Jacob, D., Teichmann, C., Remedio, A., Remke, T., Kriegsmann, A., Bülow, K., Weber, T., Buntemeyer, L., Sieck, K., and Rechid, D.: Climate hazard indices projec-

tions based on CORDEX-CORE, CMIP5 and CMIP6 ensemble, Clim. Dynam., 57, 1293–1383, https://doi.org/10.1007/s00382-021-05640-z, 2021.

Crétat, J., Pohl, B., Dieppois, B., Berthou, S., and Pergaud, J.: The Angola Low: relationship with southern African rainfall and ENSO, Clim. Dynam., 52, 1783–1803, https://doi.org/10.1007/s00382-018-4222-3, 2019.

Daron, J., Burgin, L., Janes, T., Jones, R. G., and Jack, C.: Climate process chains: Examples from southern Africa, Int. J. Climatol., 39, 4784–4797, https://doi.org/10.1002/joc.6106, 2019.

Davis-Reddy, C. L. and Vincent, K.: Climate Risk and Vulnerability: A Handbook for Southern Africa, 2nd Edn., CSIR, Pretoria, South Africa, 2017.

Denis, B., Laprise, R., and Caya, D.: Sensitivity of a regional climate model to the resolution of the lateral boundary conditions, Clim. Dynam., 20, 107–126, https://doi.org/10.1007/s00382-002-0264-6, 2003.

Desbiolles, F., Howard, E., Blamey, R. C., Barimalala, R., Hart, N. C. G., and Reason, C. J. C.: Role of ocean mesoscale structures in shaping the Angola-Low pressure system and the southern Africa rainfall, Clim. Dynam., 54, 3685–3704, https://doi.org/10.1007/s00382-020-05199-1, 2020.

Dieppois, B., Pohl, B., Crétat, J., Eden, J., Sidibe, M., New, M., Rouault, M., and Lawler, D.: Southern African summer-rainfall variability, and its teleconnections, on interannual to interdecadal timescales in CMIP5 models, Clim. Dynam., 53, 3505–3527, https://doi.org/10.1007/s00382-019-04720-5, 2019.

Diffenbaugh, N. S. and Giorgi, F.: Climate change hotspots in the CMIP5 global climate model ensemble, Climatic Change, 114, 813–822, https://doi.org/10.1007/s10584-012-0570-x, 2012.

Di Luca, A., de Elía, R., and Laprise, R.: Potential for added value in temperature simulated by high-resolution nested RCMs in present climate and in the climate change signal, Clim. Dynam., 40, 443–464, https://doi.org/10.1007/s00382-012-1384-2, 2013.

Dosio, A. and Panitz, H.-J.: Climate change projections for CORDEX-Africa with COSMO-CLM regional climate model and differences with the driving global climate models, Clim. Dynam., 46, 1599–1625, https://doi.org/10.1007/s00382-015-2664-4, 2016.

Dosio, A., Panitz, H.-J., Schubert-Frisius, M., and Lüthi, D.: Dynamical downscaling of CMIP5 global circulation models over CORDEX-Africa with COSMO-CLM: evaluation over the present climate and analysis of the added value, Clim. Dynam., 44, 2637–2661, https://doi.org/10.1007/s00382-014-2262-x, 2015.

Dosio, A., Jones, R. G., Jack, C., Lennard, C., Nikulin, G., and Hewitson, B.: What can we know about future precipitation in Africa? Robustness, significance and added value of projections from a large ensemble of regional climate models, Clim. Dynam., 53, 5833–5858, https://doi.org/10.1007/s00382-019-04900-3, 2019.

Dosio, A., Jury, M. W., Almazroui, M., Ashfaq, M., Diallo, I., Engelbrecht, F. A., Klutse, N. A. B., Lennard, C., Pinto, I., Sylla, M. B., and Tamoffo, A. T.: Projected future daily characteristics of African precipitation based on global (CMIP5, CMIP6) and regional (CORDEX, CORDEX-CORE) climate models, Clim. Dynam., 57, 3135–3158, https://doi.org/10.1007/s00382-021-05859-w, 2021.

Duan, H., Zhang, G., Wang, S., and Fan, Y.: Robust climate change research: a review on multi-model analysis, Environ. Res. Lett., 14, 033001, https://doi.org/10.1088/1748-9326/aaf8f9, 2019.

ESGF-DKRZ: https://esgf-data.dkrz.de/projects/esgf-dkrz/, last access: 1 September 2021.

Eyring, V., Bony, S., Meehl, G. A., Senior, C. A., Stevens, B., Stouffer, R. J., and Taylor, K. E.: Overview of the Coupled Model Intercomparison Project Phase 6 (CMIP6) experimental design and organization, Geosci. Model Dev., 9, 1937–1958, https://doi.org/10.5194/gmd-9-1937-2016, 2016.

Farr, T. G., Rosen, P. A., Caro, E., Crippen, R., Duren, R., Hensley, S., Kobrick, M., Paller, M., Rodriguez, E., Roth, L., Seal, D., Shaffer, S., Shimada, J., Umland, J., Werner, M., Oskin, M., Burbank, D., and Alsdorf, D.: The Shuttle Radar Topography Mission, Rev. Geophys., 45, RG2004, https://doi.org/10.1029/2005RG000183, 2007.

Funk, C., Peterson, P., Landsfeld, M., Pedreros, D., Verdin, J., Shukla, S., Husak, G., Rowland, J., Harrison, L., Hoell, A., and Michaelsen, J.: The climate hazards infrared precipitation with stations – a new environmental record for monitoring extremes, Sci. Data, 2, 150066, https://doi.org/10.1038/sdata.2015.66, 2015.

Giesen, N. van de, Hut, R., and Selker, J.: The Trans-African Hydro-Meteorological Observatory (TAHMO), WIREs Water, 1, 341–348, https://doi.org/10.1002/wat2.1034, 2014.

Giorgi, F.: Thirty Years of Regional Climate Modeling: Where Are We and Where Are We Going next?, J. Geophys. Res.-Atmos., 124, 5696–5723, https://doi.org/10.1029/2018JD030094, 2019.

Giorgi, F. and Gutowski, W. J.: Regional Dynamical Downscaling and the CORDEX Initiative, Annu. Rev. Environ. Res., 40, 467–490, https://doi.org/10.1146/annurev-environ-102014-021217, 2015.

Giorgi, F., Coppola, E., Raffaele, F., Diro, G. T., Fuentes-Franco, R., Giuliani, G., Mamgain, A., Llopart, M. P., Mariotti, L., and Torma, C.: Changes in extremes and hydroclimatic regimes in the CREMA ensemble projections, Climatic Change, 125, 39–51, https://doi.org/10.1007/s10584-014-1117-0, 2014.

Harris, I., Jones, P. D., Osborn, T. J., and Lister, D. H.: Updated high-resolution grids of monthly climatic 169 observations – the CRU TS3.10 Dataset, Int. J. Climatol., 34, 623–642, https://doi.org/10.1002/joc.3711, 2014.

Hart, N. C. G., Reason, C. J. C., and Fauchereau, N.: Tropical–Extratropical Interactions over Southern Africa: Three Cases of Heavy Summer Season Rainfall, Mon. Weather Rev., 138, 2608–2623, https://doi.org/10.1175/2010MWR3070.1, 2010.

Hersbach, H., Bell, B., Berrisford, P., Hirahara, S., Horányi, A., Muñoz-Sabater, J., Nicolas, J., Peubey, C., Radu, R., Schepers, D., Simmons, A., Soci, C., Abdalla, S., Abellan, X., Balsamo, G., Bechtold, P., Biavati, G., Bidlot, J., Bonavita, M., Chiara, G. D., Dahlgren, P., Dee, D., Diamantakis, M., Dragani, R., Flemming, J., Forbes, R., Fuentes, M., Geer, A., Haimberger, L., Healy, S., Hogan, R. J., Hólm, E., Janisková, M., Keeley, S., Laloyaux, P., Lopez, P., Lupu, C., Radnoti, G., Rosnay, P. de, Rozum, I., Vamborg, F., Villaume, S., and Thépaut, J.-N.: The ERA5 global reanalysis, Q. J. Roy. Meteor. Soc., 146, 1999–2049, https://doi.org/10.1002/qj.3803, 2020.

Houze, R. A.: Orographic effects on precipitating clouds, Rev. Geophys., 50, RG1001, https://doi.org/10.1029/2011RG000365, 2012.

Howard, E. and Washington, R.: Characterizing the Synoptic Expression of the Angola Low, J. Climate, 31, 7147–7165, https://doi.org/10.1175/JCLI-D-18-0017.1, 2018.

Howard, E. and Washington, R.: Drylines in Southern Africa: Rediscovering the Congo Air Boundary, J. Climate, 32, 8223–8242, https://doi.org/10.1175/JCLI-D-19-0437.1, 2019.

IPCC: Annex I: Atlas of Global and Regional Climate Projections, in: Climate Change 2013: The Physical Science Basis, Contribution of Working Group I to the Fifth Assessment Report of the Intergovernmental Panel on Climate Change, edited by: Stocker, T. F., Qin, D., Plattner, G.-K., Tignor, M., Allen, S. K., Boschung, J., Nauels, A., Xia, Y., Bex, V., and Midgley, P. M., Cambridge University Press, Cambridge, United Kingdom and New York, NY, USA, 1311–1394, https://doi.org/10.1017/CBO9781107415324.029, 2013.

Janowiak, J. E.: An Investigation of Interannual Rainfall Variability in Africa, J. Climate, 1, 240–255, https://doi.org/10.1175/1520-0442(1988)001<0240:AIOIRV>,2.0.CO;2, 1988.

Kalognomou, E.-A., Lennard, C., Shongwe, M., Pinto, I., Favre, A., Kent, M., Hewitson, B., Dosio, A., Nikulin, G., Panitz, H.-J., and Büchner, M.: A Diagnostic Evaluation of Precipitation in CORDEX Models over Southern Africa, J. Climate, 26, 9477–9506, https://doi.org/10.1175/JCLI-D-12-00703.1, 2013.

Karypidou, M. C.: Precipitation over southern Africa: Is there consensus among GCMs, RCMs and observational data? (Version 1), Zenodo [data set], https://doi.org/10.5281/zenodo.4725441, 2021.

Kendall, M. G.: Rank correlation methods, Griffin, Oxford, England, 1948.

Kim, J., Waliser, D. E., Mattmann, C. A., Goodale, C. E., Hart, A. F., Zimdars, P. A., Crichton, D. J., Jones, C., Nikulin, G., Hewitson, B., Jack, C., Lennard, C., and Favre, A.: Evaluation of the CORDEX-Africa multi-RCM hindcast: systematic model errors, Clim. Dynam., 42, 1189–1202, https://doi.org/10.1007/s00382-013-1751-7, 2014.

Kim, Y.-H., Min, S.-K., Zhang, X., Sillmann, J., and Sandstad, M.: Evaluation of the CMIP6 multi-model ensemble for climate extreme indices, Weather Clim. Extrem., 29, 100269, https://doi.org/10.1016/j.wace.2020.100269, 2020.

Kula, N., Haines, A., and Fryatt, R.: Reducing Vulnerability to Climate Change in Sub-Saharan Africa: The Need for Better Evidence, PLoS Med., 10, e1001374, https://doi.org/10.1371/journal.pmed.1001374, 2013.

Laprise, R., de Elía, R., Caya, D., Biner, S., Lucas-Picher, P., Diaconescu, E., Leduc, M., Alexandru, A., Separovic, L., and Canadian Network for Regional Climate Modelling and Diagnostics: Challenging some tenets of Regional Climate Modelling, Meteorol. Atmos. Phys., 100, 3–22, https://doi.org/10.1007/s00703-008-0292-9, 2008.

Le Coz, C. and van de Giesen, N.: Comparison of Rainfall Products over Sub-Saharan Africa, J. Hydrometeorol., 21, 553–596, https://doi.org/10.1175/JHM-D-18-0256.1, 2020.

L'Heureux, M. L., Lee, S., and Lyon, B.: Recent multidecadal strengthening of the Walker circulation across the tropical Pacific, Nat. Clim. Change, 3, 571–576, https://doi.org/10.1038/nclimate1840, 2013.

Lorenz, C. and Kunstmann, H.: The Hydrological Cycle in Three State-of-the-Art Reanalyses: Intercomparison and Performance Analysis, J. Hydrometeorol., 13, 1397–1420, https://doi.org/10.1175/JHM-D-11-088.1, 2012.

Lyon, B. and Mason, S. J.: The 1997–98 Summer Rainfall Season in Southern Africa. Part I: Observations, J. Climate, 20, 5134–5148, https://doi.org/10.1175/JCLI4225.1, 2007.

Mabhaudhi, T., Mpandeli, S., Nhamo, L., Chimonyo, V. G. P., Nhemachena, C., Senzanje, A., Naidoo, D., and Modi, A. T.: Prospects for Improving Irrigated Agriculture in Southern Africa: Linking Water, Energy and Food, Water, 10, 1881, https://doi.org/10.3390/w10121881, 2018.

Maidment, R. I., Grimes, D., Allan, R. P., Tarnavsky, E., Stringer, M., Hewison, T., Roebeling, R., and Black, E.: The 30 year TAMSAT African Rainfall Climatology And Time series (TARCAT) data set, J. Geophys. Res.-Atmos., 119, 10619–10644, https://doi.org/10.1002/2014JD021927, 2014.

Maidment, R. I., Allan, R. P., and Black, E.: Recent observed and simulated changes in precipitation over Africa, Geophys. Res. Lett., 42, 8155–8164, https://doi.org/10.1002/2015GL065765, 2015.

Mann, H. B.: Nonparametric Tests Against Trend, Econometrica, 13, 245–259, https://doi.org/10.2307/1907187, 1945.

Meque, A. and Abiodun, B. J.: Simulating the link between ENSO and summer drought in Southern Africa using regional climate models, Clim. Dynam., 44, 1881–1900, https://doi.org/10.1007/s00382-014-2143-3, 2015.

Munday, C. and Washington, R.: Circulation controls on southern African precipitation in coupled models: The role of the Angola Low, J. Geophys. Res. Atmospheres, 122, 861–877, https://doi.org/10.1002/2016JD025736, 2017.

Munday, C. and Washington, R.: Systematic Climate Model Rainfall Biases over Southern Africa: Links to Moisture Circulation and Topography, J. Climate, 31, 7533–7548, https://doi.org/10.1175/JCLI-D-18-0008.1, 2018.

Nikulin, G., Jones, C., Giorgi, F., Asrar, G., Büchner, M., Cerezo-Mota, R., Christensen, O. B., Déqué, M., Fernandez, J., Hänsler, A., Meijgaard, E. van, Samuelsson, P., Sylla, M. B., and Sushama, L.: Precipitation Climatology in an Ensemble of CORDEX-Africa Regional Climate Simulations, J. Climate, 25, 6057–6078, https://doi.org/10.1175/JCLI-D-11-00375.1, 2012.

Novella, N. S. and Thiaw, W. M.: African Rainfall Climatology Version 2 for Famine Early Warning Systems, J. Appl. Meteorol. Clim., 52, 588–606, https://doi.org/10.1175/JAMC-D-11-0238.1, 2013.

Onyutha, C.: Trends and variability in African long-term precipitation, Stoch. Environ. Res. Risk Ass., 32, 2721–2739, https://doi.org/10.1007/s00477-018-1587-0, 2018.

Peterson, T. C. and Manton, M. J.: Monitoring Changes in Climate Extremes: A Tale of International Collaboration, B. Am. Meteorol. Soc., 89, 1266–1271, 2008.

Pichelli, E., Coppola, E., Sobolowski, S., Ban, N., Giorgi, F., Stocchi, P., Alias, A., Belušić, D., Berthou, S., Caillaud, C., Cardoso, R. M., Chan, S., Christensen, O. B., Dobler, A., de Vries, H., Goergen, K., Kendon, E. J., Keuler, K., Lenderink, G., Lorenz, T., Mishra, A. N., Panitz, H.-J., Schär, C., Soares, P. M. M., Truhetz, H., and Vergara-Temprado, J.: The first multi-model ensemble of regional climate simulations at kilometer-scale resolution part 2: historical and future simulations of precipitation, Clim. Dynam., 56, 3581–3602, https://doi.org/10.1007/s00382-021-05657-4, 2021.

Pierce, D. W., Barnett, T. P., Santer, B. D., and Gleckler, P. J.: Selecting global climate models for regional climate change studies, P. Natl. Acad. Sci. USA, 106, 8441–8446, https://doi.org/10.1073/pnas.0900094106, 2009.

Pinto, I., Lennard, C., Tadross, M., Hewitson, B., Dosio, A., Nikulin, G., Panitz, H.-J., and Shongwe, M. E.: Evaluation and projections of extreme precipitation over southern Africa from two CORDEX models, Climatic Change, 135, 655–668, https://doi.org/10.1007/s10584-015-1573-1, 2016.

R Core Team: A language and environment for statistical computing, R Foundation for Statistical Computing, https://www.r-project.org/, last access: 31 October 2021.

Reason, C. J. C. and Jagadheesha, D.: A model investigation of recent ENSO impacts over southern Africa, Meteorol. Atmos. Phys., 89, 181–205, https://doi.org/10.1007/s00703-005-0128-9, 2005.

Rocklöv, J. and Dubrow, R.: Climate change: an enduring challenge for vector-borne disease prevention and control, Nat. Immunol., 21, 479–483, https://doi.org/10.1038/s41590-020-0648-y, 2020.

Schneider, U., Becker, A., Finger, P., Meyer-Christoffer, A., Rudolf, B., and Ziese, M.: GPCC Full Data Reanalysis Version 7.0 at 0.5°: Monthly Land-Surface Precipitation from Rain-Gauges built on GTS-based and Historic Data, Global Precipitation Climatology Centre [data set], https://doi.org/10.5676/DWD_GPCC/FD_M_V7_050, 2015.

Schulzweida, U.: CDO User Guide (Version 2.0.0), https://code.mpimet.mpg.de/projects/cdo/, last access: 31 October 2021.

Sen, P. K.: Estimates of the Regression Coefficient Based on Kendall's Tau, J. Am. Stat. Assoc., 63, 1379–1389, https://doi.org/10.1080/01621459.1968.10480934, 1968.

Serdeczny, O., Adams, S., Baarsch, F., Coumou, D., Robinson, A., Hare, W., Schaeffer, M., Perrette, M., and Reinhardt, J.: Climate change impacts in Sub-Saharan Africa: from physical changes to their social repercussions, Reg. Environ. Change, 17, 1585–1600, https://doi.org/10.1007/s10113-015-0910-2, 2017.

Tarnavsky, E., Grimes, D., Maidment, R., Black, E., Allan, R. P., Stringer, M., Chadwick, R., and Kayitakire, F.: Extension of the TAMSAT Satellite-Based Rainfall Monitoring over Africa and from 1983 to Present, J. Appl. Meteorol. Clim., 53, 2805–2822, https://doi.org/10.1175/JAMC-D-14-0016.1, 2014.

Taylor, K. E., Stouffer, R. J., and Meehl, G. A.: An Overview of CMIP5 and the Experiment Design, B. Am. Meteorol. Soc., 93, 485–498, https://doi.org/10.1175/BAMS-D-11-00094.1, 2012.

Theil, H.: A Rank-Invariant Method of Linear and Polynomial Regression Analysis, in: Henri Theil's Contributions to Economics and Econometrics: Econometric Theory and Methodology, edited by: Raj, B. and Koerts, J., Springer Netherlands, Dordrecht, 345–381, https://doi.org/10.1007/978-94-011-2546-8_20, 1992.

Tirado, M. C., Hunnes, D., Cohen, M. J., and Lartey, A.: Climate Change and Nutrition in Africa, J. Hunger Environ. Nutr., 10, 22–46, https://doi.org/10.1080/19320248.2014.908447, 2015.

Toté, C., Patricio, D., Boogaard, H., Van der Wijngaart, R., Tarnavsky, E., and Funk, C.: Evaluation of Satellite Rainfall Estimates for Drought and Flood Monitoring in Mozambique, Remote Sens., 7, 1758–1776, https://doi.org/10.3390/rs70201758, 2015.

Ukkola, A. M., Kauwe, M. G. D., Roderick, M. L., Abramowitz, G., and Pitman, A. J.: Robust Future Changes in Meteorological Drought in CMIP6 Projections Despite Uncertainty in Precipitation, Geophys. Res. Lett., 47, e2020GL087820, https://doi.org/10.1029/2020GL087820, 2020.

Warnatzsch, E. A. and Reay, D. S.: Temperature and precipitation change in Malawi: Evaluation of CORDEX-Africa climate simulations for climate change impact assessments and adaptation planning, Sci. Total Environ., 654, 378–392, https://doi.org/10.1016/j.scitotenv.2018.11.098, 2019.

Willmott, C. J. and Matsuura, K.: Smart Interpolation of Annually Averaged Air Temperature in the United States, J. Appl. Meteorol. 34, 2577–2586, https://doi.org/10.1175/1520-0450(1995)034<2577:SIOAAA>2.0.CO;2, 1995.

Wyser, K., van Noije, T., Yang, S., von Hardenberg, J., O'Donnell, D., and Döscher, R.: On the increased climate sensitivity in the EC-Earth model from CMIP5 to CMIP6, Geosci. Model Dev., 13, 3465–3474, https://doi.org/10.5194/gmd-13-3465-2020, 2020.

Xie, P. and Arkin, P. A.: Global Precipitation: A 17-Year Monthly Analysis Based on Gauge Observations, Satellite 269 Estimates, and Numerical Model Outputs, B. Am. Meteorol. Soc., 78, 2539–2558, 1997. https://doi.org/10.1175/1520-0477(1997)078<2539:GPAYMA>2.0.CO;2

Yim, B. Y., Yeh, S.-W., and Sohn, B.-J.: ENSO-Related Precipitation and Its Statistical Relationship with the Walker Circulation Trend in CMIP5 AMIP Models, Atmosphere, 7, 19, https://doi.org/10.3390/atmos7020019, 2016.